Journal of Zhejiang University SCIENCE A
ISSN 1673-565X (Print); ISSN 1862-1775 (Online)
www.zju.edu.cn/jzus; www.springerlink.com
E-mail: jzus@zju.edu.cn

Hierarchical models for failure analysis of plates bent by distributed and localized transverse loadings

Erasmo CARRERA, Gaetano GIUNTA

(*Aeronautic and Space Engineering Department, Politecnico di Torino, Torino, Italy*)

E-mail: erasmo.carrera@polito.it; gaetano.giunta@polito.it

Received May 17, 2007; revision accepted Dec. 25, 2007; published online Apr. 15, 2008

Abstract: The failure analysis of simply supported, isotropic, square plates is addressed. Attention focuses on minimum failure load amplitudes and failure locations. von Mises' equivalent stress along the plate thickness is also addressed. Several distributed and localized loading conditions are considered. Loads act on the top of the plate. Bi-sinusoidal and uniform loads are taken into account for distributed loadings, while stepwise constant centric and off-centric loadings are addressed in the case of localized loadings. Analysis is performed considering plates whose length-to-thickness ratio a/h can be as high as 100 (thin plates) and as low as 2 (very thick plates). Results are obtained via several 2D plate models. Classical theories (CTs) and higher order models are applied. Those theories are based on polynomial approximation of the displacement field. Among the higher order theories (HOTs), HOTs^{d} models account for the transverse shear deformations, while HOTs models account for both transverse shear and transverse normal deformations. LHOTs represent a local application of the higher order theories. A layerwise approach is thus assumed: by means of mathematical interfaces, the plate is considered to be made of several fictitious layers. The exact 3D solution is presented in order to determine the accuracy of the results obtained via the 2D models. In this way a hierarchy among the 2D theories is established. CTs provide highly accurate results for a/h greater than 10 in the case of distributed loadings and greater than 20 for localized loadings. Results obtained via HOTs are highly accurate in the case of very thick plates for bi-sinusoidal and centric loadings. In the case of uniform and off-centric loadings a high gradient is present in the neighborhood of the plate top. In those cases, LHOTs yield results that match the exact solution.

Key words: Failure load, von Mises' equivalent stress, Isotropic plates, Higher order theories (HOTs), Exact 3D solution
doi:10.1631/jzus.A072110 **Document code:** A **CLC number:** TU2; TU3

INTRODUCTION

The static, elastic response of plates is an important and interesting problem from both engineering and mathematical points of view. In particular, the accurate prediction of the maximum load that a plate can withstand before its failure plays a paramount role. Research activity focused and still focuses its attention on the determinations of plates failure parameters by means of several mathematical models. In (Pandey and Reddy, 1987; Reddy and Pandey, 1987; Reddy and Reddy, 1987) the finite element method has been adopted to compute the maximum value and location of the failure load for simply supported laminates under uniformly distributed bending loads and in-plane loading conditions. Analytical methods based on the closed form solution have been applied by Turvey (1980a; 1980b; 1980c; 1981; 1982; 1987) to the flexural failure analysis of composite plates and strips subjected to uniformly distributed loadings. In (Turvey, 1980a; 1980b; 1980c; 1981; 1982) classical theories (CTs) based on Cauchy (1828), Poisson (1829) and Kirchhoff (1850)'s hypotheses have been applied to compute the first-ply failure loads. In (Turvey, 1987) the shear deformation effects have been considered by means of the first shear deformation theories of Reissner (1945) and Mindlin (1951) and via the higher order shear deformation theory of Reddy (1984; 1997). In the present work failure analyses of isotropic plates have been performed

adopting several 2D, closed form, Navier type solutions. Those models have been applied in (Carrera and Giunta, 2007) to compute displacements and stresses for plates bent by localized transverse loadings. Here attention focuses on the minimum failure load that plates can withstand, on the location where failure is firstly experienced and on the von Mises' equivalent stress. First of all, CTs (Cauchy, 1828; Poisson, 1829; Kirchhoff, 1850; Reissner, 1945; Mindlin, 1951) have been assumed (see subsection "Classical theories"). In order to model the shear and transverse deformations, higher order theories (HOTs) have been considered. Those models are described in subsection "Higher order theories". In subsection "Local higher order theories" higher order models are locally applied. The whole plate is ideally divided through-the-thickness into N_l fictitious layers by means of mathematical interfaces Σ. HOTs are applied at layer level and integrity of the plate is ensured by the imposition of the displacement field congruency in the correspondence of the mathematical interfaces. Kam and Jan (1995) adopted the layerwise approach in conjunction with the finite element method for the failure analysis of composites plates. In (Kam and Jan, 1995) the displacement field is postulated to be linear through-the-thickness direction. Here the maximum order of the theories is considered to be four. Analyses have been performed considering different values for the ratio between the plate side length a and thickness h. Results vary from thin plates (a/h=100) up to very thick ones (a/h=2). Several loading conditions are presented. Distributed loadings are continuously defined above the plate top surface. For this case a bi-sinusoidal and a uniform load are addressed. Localized loadings are stepwise constant above the top of the plate. Centric and off-centric loads are considered. The exact 3D solution obtained by Demasi (2007) is employed and extended to account for the loading conditions considered in this study. Hence, benchmark results are established in order to validate the present 2D theories. Furthermore, the 2D theories presented here are hierarchically classified on the basis of their accuracy.

PRELIMINARIES

A plate of sides length a and b are considered. The plate thickness is h. The reference system is a Cartesian one with the origin at one plate corner: x and y are along the plate sides and z is the direction through the plate thickness and they are bounded between $0\leq x\leq a$, $0\leq y\leq b$ and $-h/2\leq z\leq h/2$. Plate reference surface Ω is identified by plane z=0. Plate geometry and reference system are shown in Fig.1. The notation for the displacement field is:

$$\boldsymbol{u}(x,y,z)=\begin{Bmatrix}u_x(x,y,z)\\u_y(x,y,z)\\u_z(x,y,z)\end{Bmatrix}. \tag{1}$$

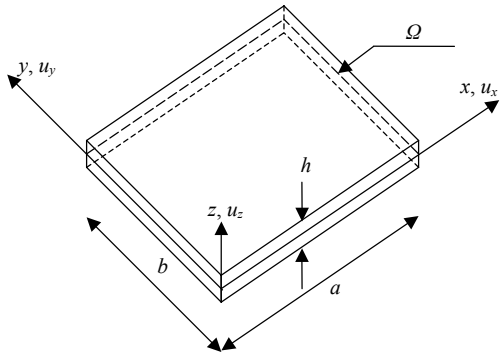

Fig.1 Plate geometry and reference system

Stress σ_{ij} (i, j=x, y, z) and strain ε_{ij} (i, j=x, y, z) components are grouped into in-plane terms $\boldsymbol{\sigma}_p$, $\boldsymbol{\varepsilon}_p$ and out-of-plane terms $\boldsymbol{\sigma}_n$, $\boldsymbol{\varepsilon}_n$:

$$\boldsymbol{\sigma}_p=\begin{Bmatrix}\sigma_{xx}\\\sigma_{yy}\\\sigma_{xy}\end{Bmatrix},\quad \boldsymbol{\sigma}_n=\begin{Bmatrix}\sigma_{xz}\\\sigma_{yz}\\\sigma_{zz}\end{Bmatrix},\quad \boldsymbol{\varepsilon}_p=\begin{Bmatrix}\varepsilon_{xx}\\\varepsilon_{yy}\\\varepsilon_{xy}\end{Bmatrix},\quad \boldsymbol{\varepsilon}_n=\begin{Bmatrix}\varepsilon_{xz}\\\varepsilon_{yz}\\\varepsilon_{zz}\end{Bmatrix}. \tag{2}$$

The plate is a linear elastic isotropic lamina and the generalized Hooke's law holds:

$$\begin{cases}\boldsymbol{\sigma}_p=\boldsymbol{C}_{pp}\boldsymbol{\varepsilon}_p+\boldsymbol{C}_{pn}\boldsymbol{\varepsilon}_n,\\ \boldsymbol{\sigma}_n=\boldsymbol{C}_{np}\boldsymbol{\varepsilon}_p+\boldsymbol{C}_{nn}\boldsymbol{\varepsilon}_n,\end{cases} \tag{3}$$

where

$$\boldsymbol{C}_{pp}=\begin{bmatrix}C_{11}&C_{12}&0\\C_{12}&C_{11}&0\\0&0&C_{66}\end{bmatrix};\ \boldsymbol{C}_{nn}=\begin{bmatrix}C_{66}&0&0\\0&C_{66}&0\\0&0&C_{11}\end{bmatrix};\ \boldsymbol{C}_{pn}=\boldsymbol{C}_{np}^{\mathrm{T}}=\begin{bmatrix}0&0&C_{12}\\0&0&C_{12}\\0&0&0\end{bmatrix}. \tag{4}$$

Coefficients C_{ij} in Eq.(4) are:

$$C_{11}=\frac{(1-\nu)E}{(1+\nu)(1-2\nu)},\ C_{12}=\frac{\nu E}{(1+\nu)(1-2\nu)},\\ C_{66}=\frac{C_{11}-C_{12}}{2}=\frac{E}{2(1+\nu)}, \tag{5}$$

where E is the Young's modulus and ν the Poisson's ratio. Under the hypothesis of small displacements, linear strain/displacement relations can be assumed:

$$\begin{cases}\boldsymbol{\varepsilon}_p=\boldsymbol{D}_p\boldsymbol{u},\\ \boldsymbol{\varepsilon}_n=(\boldsymbol{D}_{n\Omega}+\boldsymbol{D}_{nz})\boldsymbol{u}.\end{cases} \tag{6}$$

$\boldsymbol{D}_p$, $\boldsymbol{D}_{n\Omega}$ and $\boldsymbol{D}_{nz}$ are differential operators:

$$\boldsymbol{D}_p=\begin{bmatrix}\frac{\partial}{\partial x}&0&0\\0&\frac{\partial}{\partial y}&0\\\frac{\partial}{\partial y}&\frac{\partial}{\partial x}&0\end{bmatrix},\quad \boldsymbol{D}_{n\Omega}=\begin{bmatrix}0&0&\frac{\partial}{\partial x}\\0&0&\frac{\partial}{\partial y}\\0&0&0\end{bmatrix},\\ \boldsymbol{D}_{nz}=\begin{bmatrix}\frac{\partial}{\partial z}&0&0\\0&\frac{\partial}{\partial z}&0\\0&0&\frac{\partial}{\partial z}\end{bmatrix}. \tag{7}$$

CONSIDERED THEORIES

Several 2D theories have been considered. The Navier type, closed form solution is addressed. All of the theories are axiomatically formulated, that is, the displacement field has been "reasonably" postulated (Love, 1959; Washizu, 1968; Librescu, 1975). Based on the hypotheses on the displacement field, three groups of plate models have been identified: CTs, HOTs, local higher order theories (LHOTs).

Classical theories

Thin plate theories (TPTs) and First Order Shear Deformation Theory (FSDT) are pertinent to this group. TPTs are based on Cauchy (1828), Poisson (1829) and Kirchhoff (1850)'s assumption type. The displacement field is postulated such that the plate sections that are initially orthogonal to the reference surface Ω, after deformation remain orthogonal to Ω:

$$\begin{cases}u_q(x,y,z)=u_{q0}(x,y)-z\dfrac{\partial u_{z0}(x,y)}{\partial q},\quad q=x,y,\\ u_z(x,y,z)=u_{z0}(x,y),\end{cases} \tag{8}$$

where subscript 0 denotes displacement terms computed on the reference surface Ω. In that model transverse shear and through-the-thickness deformations are discarded:

$$\varepsilon_{zz}=\varepsilon_{xz}=\varepsilon_{yz}=0. \tag{9}$$

FSDT is based on Reissner (1945) and Mindlin (1951)'s theory:

$$\begin{cases}u_q(x,y,z)=u_{q0}(x,y)+zu_{q1}(x,y),\quad q=x,y,\\ u_z(x,y,z)=u_{z0}(x,y),\end{cases} \tag{10}$$

that takes into account the shear deformations but not the transversal one:

$$\varepsilon_{xz}\neq0,\ \varepsilon_{yz}\neq0,\ \varepsilon_{zz}=0. \tag{11}$$

In order to deal with the complete stress state, out-of-plane stresses σ_{iz} (i=x, y, z) have been obtained here by means of integration of the infinite equilibrium equations.

Higher order theories

A more generic displacement field can be obtained via the following polynomial approximation:

$$\begin{cases}u_q(x,y,z)=\sum_{i=0}^{N}z^iu_{qi}(x,y),\ q=x,y,\\ u_z(x,y,z)=\sum_{j=0}^{N_z}z^ju_{zj}(x,y).\end{cases} \tag{12}$$

The shear deformations are modeled via the N-order polynomial approximation of the in-plane displacement components (u_x,u_y). Also the transverse deformation is taken into account with an expansion order N_z of the transverse displacement component

higher than zero. That last term can be neglected by setting N_z=0. The acronym HOTs^{d} is used to refer to HOTs that discard the transverse deformation, while in the case of HOTs N_z=N. Results have been obtained considering N=3 and 4 for both HOTs^{d} and HOTs. Eq.(12) can be expressed in a compact form:

$$\boldsymbol{u}(x,y,z)=\sum_{\tau=0}^{N^*}F_\tau(z)\boldsymbol{u}_\tau(x,y), \tag{13}$$

where $F_\tau(z)=z^\tau$ (τ=0, 1, …, N^*) are the classical polynomial base, N^* is equal to N in the case of the in-plane displacement components and equal to N_z for the transverse component u_z. The way use to compute out-of-plane stress components σ_{iz} (i=x, y, z), discriminates between HOTs$_{ee}$, where integration of infinite equilibrium equations has been performed and HOTs$_{H}$, for which Hooke's law has been assumed.

Local higher order theories

When a layerwise approach is assumed (Carrera, 2002; 2003), the whole lamina domain D=$\{x, y\in\Omega; -h/2\le z\le h/2\}$ is ideally divided into N_l fictitious layers D_k=$\{x, y\in\Omega; -1\le\zeta_k=2z_k/h_k\le1\}$ by means of mathematical interfaces Σ (Fig.2), that is, planes parallel to the plate reference surface Ω such that:

$$\begin{cases} D=\bigcup_{k=1}^{N_l}D_k, \\ h=\sum_{k=1}^{N_l}h_k. \end{cases} \tag{14}$$

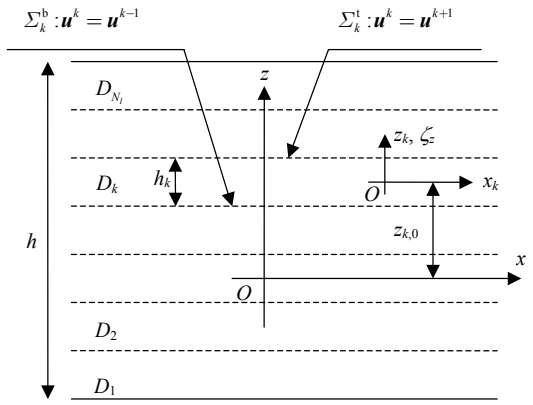

Fig.2 Division of the plate into fictitious layers

The term h_k is the distance along the thickness between two consecutive mathematical interfaces; ζ_k is the k-layer local dimensionless coordinate through-the-thickness. Its relation with the global coordinate z is shown in Fig.2. Local coordinates ζ_k=±1 identify the mathematical interfaces Σ_k^{t}, Σ_k^{b} at top and bottom of the k-layer. The displacement field is locally assumed between two consecutive interfaces, $\forall k\in\{1, 2, \ldots, N_l\}$, Eq.(15) holds:

$$\begin{cases} u_x^k(x,y,z)=\sum_{\tau=0}^{N}F_\tau(\zeta_k)u_{x\tau}^k(x,y), \\ u_y^k(x,y,z)=\sum_{\tau=0}^{N}F_\tau(\zeta_k)u_{y\tau}^k(x,y), \quad N\ge1, \\ u_z^k(x,y,z)=\sum_{\tau=0}^{N}F_\tau(\zeta_k)u_{z\tau}^k(x,y), \end{cases} \tag{15}$$

and in a compact form:

$$\boldsymbol{u}^k(x,y,z)=\sum_{\tau=0}^{N}F_\tau(\zeta_k)\boldsymbol{u}_\tau^k(x,y), \quad N\ge1. \tag{16}$$

Functions $F_\tau(\zeta_k)$ represent a polynomial expansion base different from the classical one adopted in Eq.(13). In this case a linear combination of Legendre's polynomials $P_j(\zeta_k)$ is assumed:

$$\begin{cases} F_0(\zeta_k)=[P_0(\zeta_k)-P_1(\zeta_k)]/2, \\ F_1(\zeta_k)=[P_0(\zeta_k)+P_1(\zeta_k)]/2, \\ F_r(\zeta_k)=P_r(\zeta_k)-P_{r-2}(\zeta_k), \ r=2,3,...,N, \end{cases} \tag{17}$$

where $P_j(\zeta_k)$ are defined by means of the recursive formula:

$$\begin{aligned} &P_0(\zeta_k)=1, \quad P_1(\zeta_k)=\zeta_k, -1\le\zeta_k\le1, \\ &(n+1)P_{n+1}(\zeta_k)=(2n+1)\zeta_kP_n(\zeta_k)-nP_{n-1}(\zeta_k), \\ &n=1,2,... \end{aligned} \tag{18}$$

The polynomial base in Eq.(17) has been chosen for the following properties:

$$\begin{cases} \zeta_k=1, F_1=1; F_0=0; F_r=0, \\ \zeta_k=-1, F_1=0; F_0=1; F_r=0, \\ r=2,3,...,N, \end{cases} \tag{19}$$

that satisfy the displacement field congruency in

correspondence of the mathematical interfaces $\forall k \in \{2, 3, \ldots, N_l-1\}$ (Fig.2):

$$\begin{cases} \boldsymbol{u}^k = \boldsymbol{u}^{k+1}, \ \forall (x,y) \in \Sigma_k^{\mathrm{t}} \equiv \Sigma_{k+1}^{\mathrm{b}}, \\ \boldsymbol{u}^k = \boldsymbol{u}^{k-1}, \ \forall (x,y) \in \Sigma_k^{\mathrm{b}} \equiv \Sigma_{k-1}^{\mathrm{t}}, \end{cases} \tag{20}$$

by means of:

$$\begin{cases} \boldsymbol{u}_1^k = \boldsymbol{u}_0^{k+1}, \ \forall (x,y) \in \Sigma_k^{\mathrm{t}} \equiv \Sigma_{k+1}^{\mathrm{b}}, \\ \boldsymbol{u}_0^k = \boldsymbol{u}_1^{k-1}, \ \forall (x,y) \in \Sigma_k^{\mathrm{b}} \equiv \Sigma_{k-1}^{\mathrm{t}}, \end{cases} \tag{21}$$

where $\boldsymbol{u}_1^k$ and $\boldsymbol{u}_0^k$ are the displacements vectors at k-layer top (ζ_k=1) and bottom (ζ_k=−1), respectively. LHOTs$_{\mathrm{ee}}$ stands for the assumption of the infinite equilibrium equations in order to retrieve the out-of-plane stress components, while in the case of LHOTs$_{\mathrm{H}}$ all of the components are computed by means of Hooke's law.

GOVERNING EQUATIONS

All of the considered theories can be unified considering that CTs are a peculiar case of HOTs. Also HOTs can be regarded as a particular case of LHOTs where the number of layers, N_l, is equal to the unit and the polynomial approximation along the thickness direction is performed via the classical base $F_\tau = z^\tau$ (τ=0, 1, …, N). This unifying idea has led to the assumption of the common notation in Eqs.(12) and (16). Inside a unifying environment, comparison becomes natural and a hierarchical classification can be addressed. For more details refer to (Carrera, 2002; 2003).

Considering a generic pressure $\boldsymbol{p}^k = \{p_x^k, p_y^k, p_z^k\}^{\mathrm{T}}$ acting on every mathematical interface, the governing equations are variationally obtained via the Principle of Virtual Displacements (PVD):

$$\sum_{k=1}^{N_l} \left\{ \int_{\Omega_k} \int_{h_k} \delta(\boldsymbol{\varepsilon}_p^k)^{\mathrm{T}} \boldsymbol{\sigma}_p^k + \delta(\boldsymbol{\varepsilon}_n^k)^{\mathrm{T}} \boldsymbol{\sigma}_n^k \mathrm{d}z_k \, \mathrm{d}\Omega_k - \int_{\Sigma_k^{\mathrm{b}} \bigcup \Sigma_k^{\mathrm{t}}} \delta(\boldsymbol{u}^k)^{\mathrm{T}} \boldsymbol{p}^k \mathrm{d}\Omega_k \right\} = 0. \tag{22}$$

By imposition of the Hooke's law, Eq.(3), the displacement-strain relations, Eq.(6), and the postulated displacement field, Eq.(16), the previous equation becomes:

$$\begin{aligned} &\sum_{k=1}^{N_l} \left\{ \int_{\Omega_k} \sum_{\tau=1}^{N} \sum_{s=1}^{N} \delta(\boldsymbol{u}_\tau^k)^{\mathrm{T}} \int_{h_k} F_\tau F_s \left\{ -\boldsymbol{D}_p{}^{\mathrm{T}} (\boldsymbol{C}_{pp}^k \boldsymbol{D}_p + \boldsymbol{C}_{pn}^k \right. \right. \\ &\cdot (\boldsymbol{D}_{n\Omega} + \boldsymbol{D}_{nz})) + (-\boldsymbol{D}_{n\Omega} + \boldsymbol{D}_{nz})^{\mathrm{T}} (\boldsymbol{C}_{np}^k \boldsymbol{D}_p + \boldsymbol{C}_{nn}^k (\boldsymbol{D}_{n\Omega} \\ &\left. + \boldsymbol{D}_{nz})) \right\} \mathrm{d}z_k \, \boldsymbol{u}_s^k \mathrm{d}\Omega_k + \int_{\Gamma_k} \sum_{\tau=1}^{N} \sum_{s=1}^{N} \delta(\boldsymbol{u}_\tau^k)^{\mathrm{T}} \int_{h_k} F_\tau F_s \\ &\cdot \left\{ \boldsymbol{I}_p{}^{\mathrm{T}} (\boldsymbol{C}_{pp}^k \boldsymbol{D}_p + \boldsymbol{C}_{pn}^k (\boldsymbol{D}_{n\Omega} + \boldsymbol{D}_{nz})) + \boldsymbol{I}_{n\Omega}{}^{\mathrm{T}} (\boldsymbol{C}_{np}^k \cdot \boldsymbol{D}_p \right. \\ &\left. \left. + \boldsymbol{C}_{nn}^k (\boldsymbol{D}_{n\Omega} + \boldsymbol{D}_{nz})) \right\} \mathrm{d}z_k \, \boldsymbol{u}_s^k \mathrm{d}\Omega_k \right. \\ &\left. - \int_{\Sigma_k^{\mathrm{b}} \bigcup \Sigma_k^{\mathrm{t}}} \sum_{\tau=1}^{N} \sum_{s=1}^{N} \delta \{\boldsymbol{u}_\tau^k\}^{\mathrm{T}} \boldsymbol{p}_\tau^k \mathrm{d}\Omega_k \right\} = 0, \end{aligned} \tag{23}$$

where Γ_k is the frontier of Ω_k and $\boldsymbol{p}_\tau^k$ is a load vector variationally consistent to the applied loading conditions and:

$$\boldsymbol{I}_p = \begin{bmatrix} 1 & 0 & 0 \\ 0 & 1 & 0 \\ 1 & 1 & 0 \end{bmatrix}, \quad \boldsymbol{I}_{n\Omega} = \begin{bmatrix} 0 & 0 & 1 \\ 0 & 0 & 1 \\ 0 & 0 & 0 \end{bmatrix}. \tag{24}$$

The differential governing equations and the boundary conditions are obtained via a suitable choice of the virtual displacements $\delta(\boldsymbol{u}_\tau^k)$:

$$\begin{cases} \boldsymbol{K}^{k\tau s} \boldsymbol{u}_s^k = \boldsymbol{p}_\tau^k, \\ \boldsymbol{u}_s^k = \bar{\boldsymbol{u}}_s^k, & (x,y,z) \in \Gamma_k^*, \\ \boldsymbol{\Pi}^{k\tau s} \boldsymbol{u}_s^k = \boldsymbol{\Pi}^{k\tau s} \bar{\boldsymbol{u}}_s^k, & (x,y,z) \in \Gamma_k^{**}, \end{cases} \tag{25}$$

where Γ_k^* and Γ_k^{**} are the regions where geometrical and mechanical boundary conditions hold; $\boldsymbol{K}^{k\tau s}$ and $\boldsymbol{\Pi}^{k\tau s}$ are two differential matrices defined as follows:

$$\begin{aligned} \boldsymbol{K}^{k\tau s} = \int_{h_k} F_\tau F_s \left\{ -\boldsymbol{D}_p{}^{\mathrm{T}} (\boldsymbol{C}_{pp}^k \boldsymbol{D}_p + \boldsymbol{C}_{pn}^k (\boldsymbol{D}_{n\Omega} + \boldsymbol{D}_{nz})) \right. \\ \left. + (-\boldsymbol{D}_{n\Omega} + \boldsymbol{D}_{nz})^{\mathrm{T}} (\boldsymbol{C}_{np}^k \boldsymbol{D}_p + \boldsymbol{C}_{nn}^k (\boldsymbol{D}_{n\Omega} + \boldsymbol{D}_{nz})) \right\} \mathrm{d}z_k, \end{aligned} \tag{26}$$

$$\begin{aligned}\boldsymbol{\Pi}^{k\tau s} = \int_{h_k} F_\tau F_s \Big\{ & \boldsymbol{I}_p{}^{\mathrm{T}} (\boldsymbol{C}_{pp}^k \boldsymbol{D}_p + \boldsymbol{C}_{pn}^k (\boldsymbol{D}_{n\Omega} + \boldsymbol{D}_{nz})) \\ & + \boldsymbol{I}_{n\Omega}{}^{\mathrm{T}} (\boldsymbol{C}_{np}^k \boldsymbol{D}_p + \boldsymbol{C}_{nn}^k (\boldsymbol{D}_{n\Omega} + \boldsymbol{D}_{nz})) \Big\} \mathrm{d}z_k .\end{aligned} \tag{27}$$

Navier type, closed form solution is obtained considering harmonic displacements and loadings:

$$\begin{cases} (u_{xs}^k, p_{x\tau}^k) = \sum_{l=1}^{L} \sum_{m=1}^{M} (U_{xs}^k, P_{x\tau}^k) \cos(l\pi x / a) \sin(m\pi y / b), \\ (u_{ys}^k, p_{y\tau}^k) = \sum_{l=1}^{L} \sum_{m=1}^{M} (U_{ys}^k, P_{y\tau}^k) \sin(l\pi x / a) \cos(m\pi y / b), \\ (u_{zs}^k, p_{z\tau}^k) = \sum_{l=1}^{L} \sum_{m=1}^{M} (U_{zs}^k, P_{z\tau}^k) \sin(l\pi x / a) \sin(m\pi y / b), \\ \tau, s = 0, 1, ..., N. \end{cases} \tag{28}$$

CONSIDERED FAILURE PARAMETERS

According to the von Mises' criterion, failure is due to the distortion strain energy associated with the deviatoric stress tensor. Failure occurs when that energy reaches the yielding level required in uniaxial loading. In this case it is possible to define, in a generic Cartesian reference system, a stress level (σ_{eq}) equivalent to a general 3D stress field:

$$\begin{aligned}\sigma_{\mathrm{eq}} = \Big[& \sigma_{xx}^2 + \sigma_{yy}^2 + \sigma_{zz}^2 - \sigma_{xx}\sigma_{yy} - \sigma_{xx}\sigma_{zz} \\ & - \sigma_{yy}\sigma_{zz} + 3(\tau_{xy}^2 + \tau_{xz}^2 + \tau_{yz}^2) \Big]^{1/2} .\end{aligned} \tag{29}$$

That equivalent stress has to be compared to the admissible yielding stress σ_y. If no safety margin is taken into account, failure occurs when the ratio (This is not the unique way of defining the failure index. Also the difference between σ_{eq} and σ_y, for example, could be adopted) of σ_{eq} and σ_y is equal to or greater than the unit:

$$\sigma_{\mathrm{eq}} / \sigma_y \geq 1. \tag{30}$$

Given a reference pressure load p_{zz}^0 and the related stress field $\sigma_{ij}^0 (i, j = x, y, z)$ the stress state associated with any other value of the external pressure p_{zz} can be obtained, due to the problem linearity as follows:

$$\sigma_{ij} = \frac{p_{zz}}{p_{zz}^0} \sigma_{ij}^0, \quad i, j = x, y, z. \tag{31}$$

The expression for the minimum failure load p_{zz}^{F} can be obtained from Eqs.(29) and (31) by imposition of the failure condition in Eq.(30):

$$p_{zz}^{\mathrm{F}} = \frac{p_{zz}^0}{\sigma_{\mathrm{eq}}^0} \sigma_y . \tag{32}$$

NUMERICAL RESULTS AND DISCUSSION

In this section the analysis of plates under different loading conditions is presented. In all of the cases plates have the same geometry and they are made of the same isotropic material: aluminum alloy 7075-T651. The length-to-thickness ratio, a/h, has been chosen as analysis parameter. Geometrical data are reported in Table 1 while Table 2 lists the material mechanical properties. The condition of minimum failure load is investigated along the following points:

$$(x_i, y_j, z_l / h): \begin{cases} x_i = ia/4, & i = 0, 1, ..., 4, \\ y_i = jb/4, & j = 0, 1, ..., 4, \\ z_l / h = \pm l / 10, & l = 0, 1, ..., 5, \end{cases} \tag{33}$$

where z/h is the dimensionless coordinate along the plate thickness. Results obtained via the 2D theories are assessed by means of the exact 3D solution obtained by Demasi (2007). Using the solution method suggested in (Demasi, 2007), the von Mises' stress and the failure load are here computed for the addressed loading conditions. A hierarchy among the 2D theories is established in terms of the accuracy of the results. Concerning distributed loadings, in subsection "Distributed loadings" bi-sinusoidal and uniform loadings are considered. For uniform loadings L=M=61 in Eq.(28). In subsection "Localized loadings", centric and off-centric stepwise loadings are addressed where L=M=25. In all of the cases the loading is applied at the top of the plate.

Table 1 Plate geometrical data

Plate geometry	Value
a	300 mm
b	300 mm
a/h	100, 50, 20, 10, 5, 2

Table 2 Aluminum alloy 7075-T651 mechanical data

Material mechanical property	Value
Poisson's ratio ν	0.33
Young's modulus E	71700 N/mm^2
Yield stress σ_y	503 N/mm^2

Distributed loadings

In Table 3 the minimum failure load amplitudes and locations computed by means of the exact 3D theory are presented. In the case of bi-sinusoidal loading (Fig.3), failure is experienced at the bottom of the plate center for every considered value of the thickness parameter a/h, due to the normal stress components σ_{xx}, σ_{yy} and σ_{zz}. When a uniform loading is applied (Fig.4), the corners of the plate fail first. The location along the thickness depends on the value of the length-to-thickness ratio. For $a/h\geq10$ the bottom of the plate fails, while the top experiences the failure when a/h=5 and 2, as the uniform loading failure is due to the τ_{xy} stress component. Results obtained via the CTs models are presented in Table 4.

Also the percentage absolute errors with respect to the exact solution are reported in the case of failure locations coincident with the exact solution. For the uniform loading and $a/h\geq5$ failure is predicted to

Table 3 Minimum failure load amplitudes (N/mm^2) and locations for distributed loadings via exact 3D solution

a/h	Bi-sinusoidal loading	Uniform loading
100	2.4883×10^{-1}	1.5567×10^{-1}
	center, bot.	corners, bot.
50	9.9511×10^{-1}	6.2241×10^{-1}
	center, bot.	corners, bot.
20	6.2109	3.8827
	center, bot.	corners, bot.
10	2.4727×10^{1}	1.5469×10^{1}
	center, bot.	corners, bot.
5	9.7308×10^{1}	5.8649×10^{1}
	center, bot.	corners, top
2	5.9126×10^{2}	2.1558×10^{2}
	center, bot.	corners, top

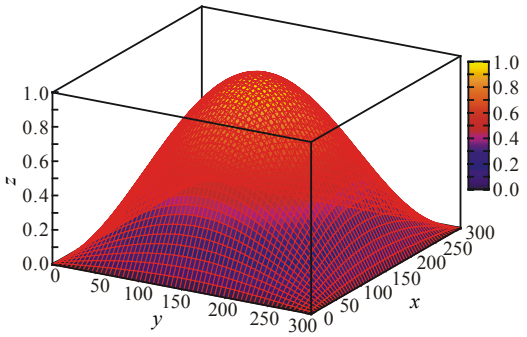

Fig.3 Bi-sinusoidal loading, L=M=1. x and y are plates' side lengths, mm; z is the load amplitude of p_{zz}, N/mm^2

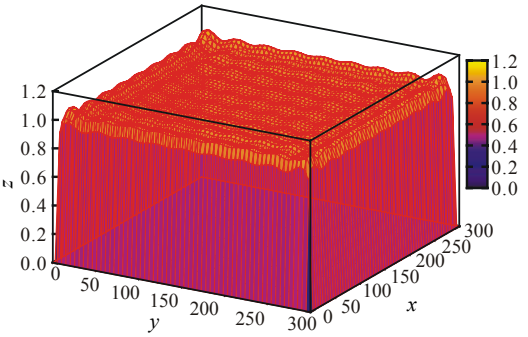

Fig.4 Uniform load via Fourier's series approximations, L=M=61. x and y are plates' side lengths, mm; z is the load amplitude of p_{zz}, N/mm^2

Table 4 Minimum failure load amplitudes (N/mm^2), locations and absolute percentage errors for distributed loadings via CTs (TPT and FSDT)

a/h	Bi-sinusoidal loading	Uniform loading
100	2.4884×10^{-1}	1.5570×10^{-1}
	center, bot.	corners, b/t**
	0.007%	0.020%
50	9.9537×10^{-1}	6.2281×10^{-1}
	center, bot.	corners, b/t
	0.026%	0.065%
20	6.2211	3.8926
	center, bot.	corners, b/t
	0.163%	0.254%
10	2.4884×10^{1}	1.5570×10^{1}
	center, bot.	corners, b/t
	0.636%	0.655%
5	9.9537×10^{1}	6.2281×10^{1}
	center, bot.	corners, b/t
	2.291%	6.194%
2	6.0823×10^{2}	2.8947×10^{2}
	H^*, 0	H, 0
	–	–

* H={(0, b/2), (a, b/2), (a/2, 0), (a/2, b)}; ** Minimum at plate top and bottom, z/h=±0.5

occur at the same time at the bottom and at the top of the plate. CTs yield highly accurate results for $a/h \geq 10$. For thick plates (a/h=5) good results are obtained, while in the case of very thick plates (a/h=2) failure locations for both distributed loading conditions differ from the exact solution. Failure is predicted to occur in the points in the set H={(0, b/2), (a, b/2), (a/2, b), (a/2, b)}. Table 5 presents results obtained considering the transverse deformability. The even polynomial terms for the approximation of the in-plane displacement components are not relevant. For very thick plates the failure location is correctly predicted in the case of N=3 and 4, while the failure load amplitudes are not accurate. For the uniform loading and a/h=20 and 10, cubic and fourth order polynomials yield results that are less accurate than those obtained by employing N=1 and 2. Fig.5 shows the von Mises' stress computed via the exact solution and HOTs^{d} models with respect to the dimensionless coordinate z/h at plate center. The amplitude of the applied load equals that of the 3D failure load for a/h=10. Tables 6 and 7 show the results and the percentage absolute errors obtained via HOTs$_{ee}$ and HOTs$_{H}$, respectively. The third and forth order theories have been considered. In the case of bi-sinusoidal loading the integration of the indefinite equilibrium equations yields correct prediction of the failure location for any considered value of the length-to-thickness ratio. HOTs$_{H}$ with N=3 do not predict the failure location for very thick plates, due to the fact that Hooke's relations have been applied to compute the out-of-plane stress components. In the case of N=4 and both HOTs$_{ee}$ and HOTs$_{H}$, results match the exact solution. In the case of uniform loading, for a/h=5 and 2 the failure locations are not

Table 5 Minimum failure load amplitudes (N/mm^2), locations and absolute percentage errors for distributed loadings via HOTs$^{d}_{ee}$ and HOTs$^{d}_{H}$

a/h	Bi-sinusoidal loading		Uniform loading	
	N=1, 2	N=3, 4	N=1, 2	N=3, 4
100	2.4884×10^{-1}	2.4882×10^{-1}	1.5570×10^{-1}	1.5565×10^{-1}
	center, bot.	center, bot.	corners, b/t**	corners, b/t
	0.007%	0.003%	0.020%	0.012%
50	9.9537×10^{-1}	9.9498×10^{-1}	6.2281×10^{-1}	6.2205×10^{-1}
	center, bot.	center, bot.	corners, b/t	corners, b/t
	0.026%	0.013%	0.065%	0.057%
20	6.2211	6.2058	3.8926	3.8661
	center, bot.	center, bot.	corners, b/t	corners, b/t
	0.163%	0.082%	0.254%	0.429%
10	2.4884×10^{1}	2.4643×10^{1}	1.5570×10^{1}	1.5212×10^{1}
	center, bot.	center, bot.	corners, b/t	corners, b/t
	0.636%	0.338%	0.655%	1.658%
5	9.9537×10^{1}	9.5835×10^{1}	6.2281×10^{1}	5.7876×10^{1}
	center, bot.	center, bot.	corners, b/t	corners, b/t
	2.291%	1.514%	6.194%	1.318%
2	6.0823×10^{2}	5.0903×10^{2}	2.8947×10^{2}	2.9463×10^{2}
	H*, 0	center, bot.	H, 0	corners, b/t
	–	13.908%	–	36.668%

* H={(0, b/2), (a, b/2), (a/2, 0), (a/2, b)}; ** Minimum at plate top and bottom, z/h=±0.5

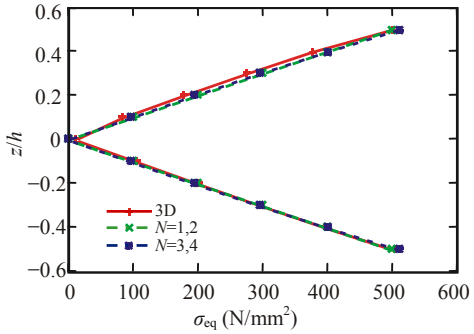

Fig.5 von Mises' stress along thickness at plate corners via exact solution and HOTs^{d} for uniform loading equal to 3D failure load, a/h=10

Table 6 Minimum failure load amplitudes (N/mm^2), locations and absolute percentage errors for distributed loadings via HOTs$_{ee}$

a/h	Bi-sinusoidal loading		Uniform loading	
	N=3	N=4	N=3	N=4
100	2.4881×10^{-1}	2.4883×10^{-1}	1.5567×10^{-1}	1.5567×10^{-1}
	center, bot.	center, bot.	corners, bot.	corners, bot.
	0.006%	0.000%	0.000%	0.000%
50	9.9486×10^{-1}	9.9511×10^{-1}	6.2242×10^{-1}	6.2241×10^{-1}
	center, bot.	center, bot.	corners, bot.	corners, bot.
	0.026%	0.000%	0.002%	0.000%
20	6.2011	6.2109	3.8820	3.8830
	center, bot.	center, bot.	corners, bot.	corners, bot.
	0.159%	0.000%	0.019%	0.007%
10	2.4572×10^{1}	2.4727×10^{1}	1.5423×10^{1}	1.5495×10^{1}
	center, bot.	center, bot.	corners, bot.	corners, bot.
	0.628%	0.000%	0.296%	0.166%
5	9.4975×10^{1}	9.7310×10^{1}	6.0428×10^{1}	6.2286×10^{1}
	center, bot.	center, bot.	corners, bot.	corners, bot.
	2.397%	0.003%	–	–
2	5.2032×10^{2}	5.9588×10^{2}	2.6304×10^{2}	2.8976×10^{2}
	center, bot.	center, bot.	H*, 0.3	H, 0.3
	11.998%	0.781%	–	–

* H={(0, b/2), (a, b/2), (a/2, 0), (a/2, b)}

correctly predicted. In Figs.6 and 7 the von Mises' stress computed via $HOTs_{ee}$ and the exact solution are compared in the cases of bi-sinusoidal loading with a/h=2 and uniform loading with a/h=5. Fig.6 shows a high stress gradient along the thickness direction in the neighbourhood of the top of the plate. Results shown in table 8 and 9 have been obtained using $LHOTs_{ee}$. The plate has been split into two and four layers respectively. Failure location for N=3 and N_l=2 is predicted in a different location than the exact one. Also for N=4 results do not properly match the exact solution, due to the fact that a high stress gradient is present for $0.4 \le z/h \le 0.5$ as shown in Figs.8 and 9. Table 10 presents results for a very thick plate with N_l=3 and 4, where a mathematical interface is located at z/h=0.4 and the remaining part of the plate is split into fictitious layers of equal thickness. Highly accurate results are then obtained.

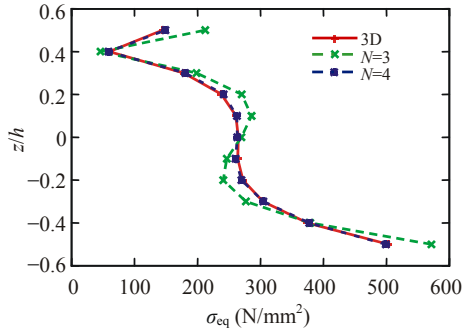

Fig.6 von Mises' stress along thickness at plate center via exact solution and HOTs for bi-sinusoidal loading equal to 3D failure load, a/h=2

Table 7 Minimum failure load amplitudes (N/mm^2), locations and absolute percentage errors for distributed loadings via $HOTs_H$

a/h	Bi-sinusoidal loading		Uniform loading	
	N=3	N=4	N=3	N=4
100	2.4884×10^{-1}	2.4883×10^{-1}	1.5567×10^{-1}	1.5567×10^{-1}
	center, bot.	center, bot.	corners, bot.	corners, bot.
	0.007%	0.000%	0.000%	0.000%
50	9.9537×10^{-1}	9.9511×10^{-1}	6.2242×10^{-1}	6.2241×10^{-1}
	center, bot.	center, bot.	corners, bot.	corners, bot.
	0.029%	0.000%	0.002%	0.000%
20	6.2212	6.2109	3.8820	3.8830
	center, bot.	center, bot.	corners, bot.	corners, bot.
	0.181%	0.000%	0.019%	0.007%
10	2.4890×10^{1}	2.4727×10^{1}	1.5423×10^{1}	1.5495×10^{1}
	center, bot.	center, bot.	corners, bot.	corners, bot.
	0.716%	0.000%	0.296%	0.166%
5	9.9912×10^{1}	9.7305×10^{1}	6.0428×10^{1}	6.2286×10^{1}
	center, bot.	center, bot.	corners, bot.	corners, bot.
	2.755%	0.002%	–	–
2	6.3392×10^{2}	5.8691×10^{2}	3.0016×10^{2}	3.3202×10^{2}
	H^*, 0	center, bot.	K^{**}, top	K, top
	–	0.736%	–	–

* H={(0, b/2), (a, b/2), (a/2, 0), (a/2, b)}; ** K={x=0, a; y=b/4, 3b/4} ∪{x=a/4, 3a/4; y=0, b}

Localized loadings

The considered stepwise localized loadings are shown in Figs.10 and 11. The centric loading is applied on {$a/3 \le x \le 2a/3$, $b/3 \le y \le 2b/3$}, while the off-centric one is defined on {$a/12 \le x \le a/4$,

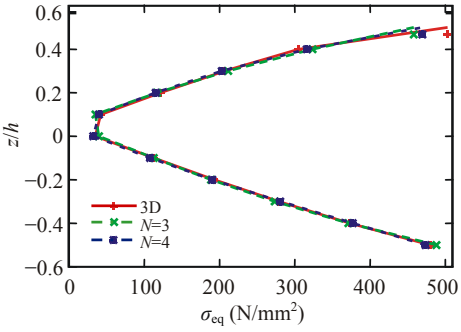

Fig.7 von Mises' stress along thickness at plate corners by 3D and HOTs for uniform loading equal to 3D failure load, a/h=5

Table 8 Minimum failure load amplitudes (N/mm^2), locations and absolute percentage errors for distributed loadings via $LHOTs_{ee}$, N_l=2

a/h	Bi-sinusoidal loading		Uniform loading	
	N=3	N=4	N=3	N=4
100	2.4882×10^{-1}	2.4883×10^{-1}	1.5567×10^{-1}	1.5567×10^{-1}
	center, bot.	center, bot.	corners, bot.	corners, bot.
	0.001%	0.000%	0.000%	0.000%
50	9.9508×10^{-1}	9.9511×10^{-1}	6.2241×10^{-1}	6.2241×10^{-1}
	center, bot.	center, bot.	corners, bot.	corners, bot.
	0.003%	0.000%	0.000%	0.000%
20	6.2097	6.2109	3.8827	3.8827
	center, bot.	center, bot.	corners, bot.	corners, bot.
	0.020%	0.000%	0.000%	0.000%
10	2.4707×10^{1}	2.4727×10^{1}	1.5469×10^{1}	1.5469×10^{1}
	center, bot.	center, bot.	corners, bot.	corners, bot.
	0.080%	0.000%	0.000%	0.000%
5	9.6997×10^{1}	9.7304×10^{1}	6.1513×10^{1}	6.0708×10^{1}
	center, bot.	center, bot.	corners, bot.	corners, top
	0.319%	0.004%	–	3.511%
2	5.8024×10^{2}	5.9061×10^{2}	2.9497×10^{2}	3.0210×10^{2}
	center, bot.	center, bot.	H^*, 0.4	corners, top
	1.865%	0.111%	–	40.130%

* H={(0, b/2), (a, b/2), (a/2, 0), (a/2, b)}

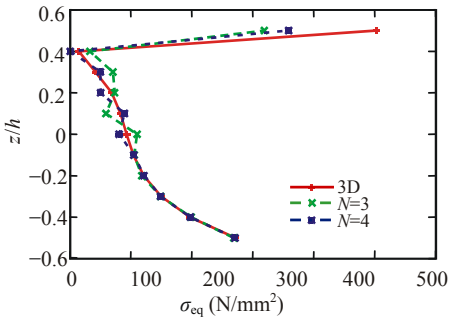

Fig.8 von Mises' stress along thickness at plate corners by 3D and LHOTs, N_l=2, for uniform loading equal to 3D failure load, a/h=2

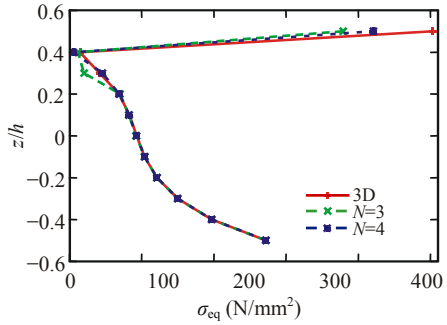

Fig.9 von Mises' stress along thickness at plate corners by 3D solution and LHOTs, N_l=4, for uniform loading equal to 3D failure load, a/h=2

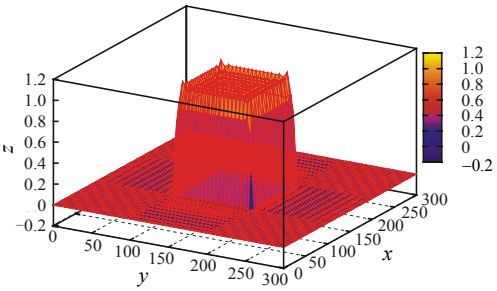

Fig.10 Centric localized loading at {$a/3\le x\le 2a/3$, $b/3\le y\le 2b/3$} via Fourier's series approximation, M=N=25. x and y are plates' side lengths, mm; z is the load amplitude of p_{zz}, N/mm²

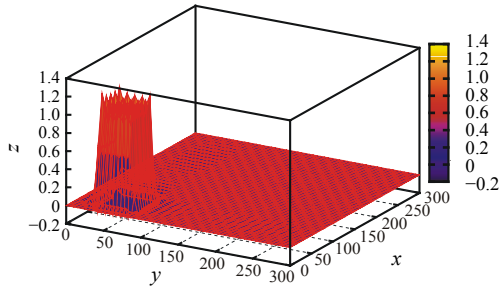

Fig.11 Off-centric localized loading at {$a/12\le x\le a/4$, $b/12\le y\le b/4$} via Fourier's series approximation, M=N=25. x and y are plates' side lengths, mm; z is the load amplitude of p_{zz}, N/mm²

Table 9 Minimum failure load amplitudes (N/mm²), locations and absolute percentage errors for distributed loadings via LHOTs$_{ee}$, N_l=4

a/h	Bi-sinusoidal loading		Uniform loading	
	N=3	N=4	N=3	N=4
100	2.4883×10^{-1}	2.4883×10^{-1}	1.5567×10^{-1}	1.5567×10^{-1}
	center, bot.	center, bot.	corners, bot.	corners, bot.
	0.000%	0.000%	0.000%	0.000%
50	9.9511×10^{-1}	9.9511×10^{-1}	6.2241×10^{-1}	6.2241×10^{-1}
	center, bot.	center, bot.	corners, bot.	corners, bot.
	0.000%	0.000%	0.000%	0.000%
20	6.2108	6.2109	3.8827	3.8827
	center, bot.	center, bot.	corners, bot.	corners, bot.
	0.002%	0.000%	0.000%	0.000%
10	2.4724×10^{1}	2.4727×10^{1}	1.5469×10^{1}	1.5469×10^{1}
	center, bot.	center, bot.	corners, bot.	corners, bot.
	0.010%	0.000%	0.000%	0.000%
5	9.7267×10^{1}	9.7308×10^{1}	6.0140×10^{1}	5.9181×10^{1}
	center, bot.	center, bot.	corners, top	corners, top
	0.042%	0.000%	2.542%	0.907%
2	5.8948×10^{2}	5.9119×10^{2}	2.8596×10^{2}	2.5759×10^{2}
	center, bot.	center, bot.	corners, top	corners, top
	0.301%	0.012%	32.643%	19.483%

Table 10 Minimum failure load amplitudes (N/mm²), locations and absolute percentage errors for distributed loadings via LHOTs$_{ee}$, a/h=2, asymmetric layers

N_l	Uniform loading	
	N=3	N=4
3	2.2491×10^{2}	2.1761×10^{2}
	corners, top	corners, top
	4.327%	0.939%
4	2.2178×10^{2}	2.1660×10^{2}
	corners, top	corners, top
	2.876%	0.471%

Table 11 Minimum failure load amplitudes (N/mm²) and locations for localized loadings via exact 3D solution

a/h	Centric loading	Off-centric loading
100	4.6222×10^{-1}	1.8901
	center, bot.	(0,0), bot.
50	1.8482	7.554
	center, bot.	(0,0), bot.
20	1.1521×10^{1}	4.6934×10^{1}
	center, bot.	(0,0), bot.
10	4.5652×10^{1}	1.8385×10^{2}
	center, bot.	(0,0), bot.
5	1.7806×10^{2}	7.1613×10^{2}
	center, bot.	(0,0), bot.
2	9.0968×10^{2}	1.3447×10^{3}
	center, 0.2	(a/4,b/4), 0.4

$b/12 \le y \le b/4\}$. According to the exact 3D solution, shown in Table 11, failure occurs at plate center in the case of centric localized load. The position along the thickness depends on the value of the thickness parameter. For $a/h \ge 5$ the bottom of the plate first fails. In the case of very thick plates failure occurs for $z/h=0.2$. About the off-centric localized loading, for $a/h \ge 5$ failure is experienced at the bottom of the corner point (0, 0). For $a/h=2$ failure is located at the first quarter point ($a/4$, $b/4$) at $z/h=0.4$. Results obtained via CTs are reported in Table 12. CTs yield highly accurate results for $a/h \ge 20$. For $a/h=10$ and 5 the absolute percentage error is acceptable. In the case of very thick plates failure locations are not correctly predicted. HOTs^{d} theories with $N=3$ and 4 provide more accurate results as shown in Table 13. The only exception is represented by the case $a/h=5$, $N=3$ and 4 for off-centric loading. For this last case, the von Mises' stress behaviour along the thickness is depicted in Fig.12 where the exact solution is also shown. Results obtained via HOTs are reported in Tables 14 and 15. In the case of centric loading and very thick plates, failure location is correctly predicted by HOT_{ee} with $N=3$ and 4 and by HOT_h with $N=4$. Fourth order polynomial approximation provides good accuracy of the results. Fig.13 shows the von Mises' equivalent stress along the thickness direction. For the off-centric loading and $a/h=2$, the correct failure location is predicted by HOT_{ee}, $N=4$, where the absolute percentage error is about 12%. The von Mises' stress computed by means of HOT_{ee}, $N=4$ is compared to the exact solution in Fig.14. A high stress gradient is present at the neighborhood of the plate top. Tables 16 and 17 present results obtained via LHOTs with $N_l=2$ and 4, respectively. Highly accurate results are obtained in the case of centric localized loading. Good agreement with the exact solution is obtained in the case of very thick plates for

Table 12 Minimum failure load amplitudes (N/mm^2), locations and absolute percentage errors for distributed loadings via CTs (TPT and FSDT)

a/h	Centric loading	Off-centric loading
100	4.6227×10^{-1}	1.8906
	center, bot.	(0,0), b/t*
	0.012%	0.028%
50	1.8491	7.5626
	center, bot.	(0,0), b/t
	0.047%	0.113%
20	1.1557×10^{1}	4.7266×10^{1}
	center, bot.	(0,0), b/t
	0.311%	0.708%
10	4.6227×10^{1}	1.8906×10^{2}
	center, bot.	(0,0), b/t
	1.260%	2.837%
5	1.8491×10^{2}	7.5626×10^{2}
	center, bot.	(0,0), b/t
	3.844%	5.603%
2	9.8335×10^{2}	2.6173×10^{3}
	center, top	(a/4,b/4), 0.1
	–	–

* Minimum at plate top and bottom, $z/h=\pm0.5$

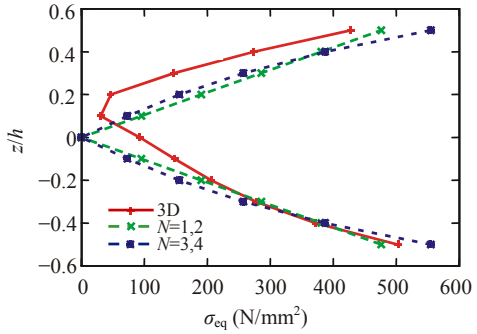

Fig.12 von Mises' stress along thickness at (0, 0) via exact solution and HOTs^{d} for off-centric loading equal to 3D failure load, $a/h=5$

Table 13 Minimum failure load amplitudes (N/mm^2), locations and absolute percentage errors for distributed loadings via HOTs$^{d}_{ee}$

a/h	Centric loading		Off-centric loading	
	N=1, 2	N=3, 4	N=1, 2	N=3, 4
100	4.6227×10^{-1}	4.6219×10^{-1}	1.8906	1.8899
	center, bot.	center, bot.	(0,0), b/t*	(0,0), b/t
	0.001%	0.006%	0.028%	0.014%
50	1.8491	1.8478	7.5626	7.5498
	center, bot.	center, bot.	(0,0), b/t	(0,0), b/t
	0.047%	0.022%	0.113%	0.056%
20	1.1557×10^{1}	1.1506×10^{1}	4.7266×10^{1}	4.6772×10^{1}
	center, bot.	center, bot.	(0,0), b/t	(0,0), b/t
	0.311%	0.126%	0.708%	0.345%
10	4.6227×10^{1}	4.5419×10^{1}	1.8906×10^{2}	1.8140×10^{2}
	center, bot.	center, bot.	(0,0), b/t	(0,0), b/t
	1.260%	0.511%	2.837%	1.332%
5	1.8491×10^{2}	1.7252×10^{2}	7.5626×10^{2}	6.4886×10^{2}
	center, bot.	center, bot.	(0,0), b/t	(0,0), b/t
	3.844%	3.116%	5.603%	9.394%
2	9.8335×10^{2}	7.9412×10^{2}	2.6173×10^{3}	2.3264×10^{3}
	center, top	center, 0.3	(a/4,b/4), 0.1	(a/4,b/4), 0.3
	–	–	–	–

* Minimum at plate top and bottom, $z/h=\pm0.5$

Table 14 Minimum failure load amplitudes (N/mm^2), locations and absolute percentage errors for distributed loadings via HOTs$_{ee}$

a/h	Centric loading		Off-centric loading	
	N=3	N=4	N=3	N=4
100	4.6217×10^{-1}	4.6222×10^{-1}	1.8901	1.8901
	center, bot.	center, bot.	(0,0), bot.	(0,0), bot.
	0.011%	0.000%	0.000%	0.000%
50	1.8474	1.8482	7.554	7.554
	center, bot.	center, bot.	(0,0), bot.	(0,0), bot.
	0.045%	0.000%	0.000%	0.000%
20	1.1488×10^{1}	1.1521×10^{1}	4.6934×10^{1}	4.6934×10^{1}
	center, bot.	center, bot.	(0,0), bot.	(0,0), bot.
	0.282%	0.000%	0.000%	0.000%
10	4.5148×10^{1}	4.5631×10^{1}	1.8379×10^{2}	1.8384×10^{2}
	center, bot.	center, bot.	(0,0), bot.	(0,0), bot.
	1.104%	0.045%	0.032%	0.005%
5	1.7088×10^{2}	1.7713×10^{2}	7.2738×10^{2}	7.1704×10^{2}
	center, bot.	center, bot.	(0,0), bot.	(0,0), bot.
	4.033%	0.526%	1.570%	0.127%
2	8.2959×10^{2}	8.8568×10^{2}	1.1960×10^{3}	1.1751×10^{3}
	center, 0.2	center, 0.2	(a/4,b/4), 0.3	(a/4,b/4), 0.4
	8.804%	2.638%	–	12.615%

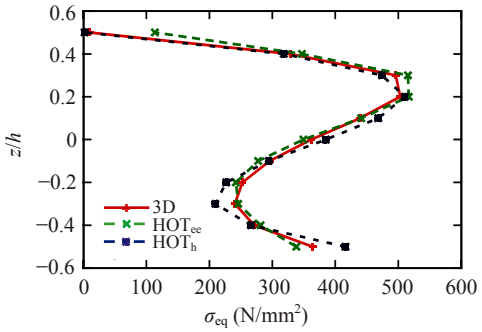

Fig.13 von Mises' stress along thickness at plate center via exact solution and HOT, N=4 for centric loading equal to 3D failure load, a/h=2

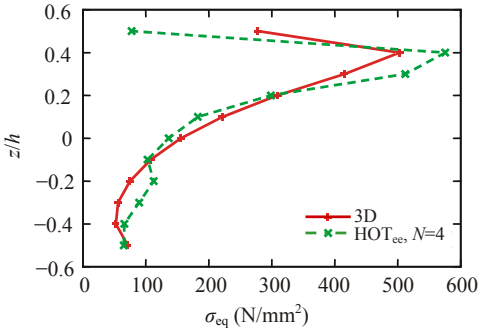

Fig.14 von Mises' stress along thickness at (a/4, b/4) via exact solution and HOT$_{ee}$, N=4 for off-centric loading equal to 3D failure load, a/h=2

Table 15 Minimum failure load amplitudes (N/mm^2), locations and absolute percentage errors for distributed loadings via HOTs$_{H}$

a/h	Centric loading		Off-centric loading	
	N=3	N=4	N=3	N=4
100	4.6227×10^{-1}	4.6222×10^{-1}	1.8901	1.8901
	center, bot.	center, bot.	(0,0), bot.	(0,0), bot.
	0.012%	0.000%	0.000%	0.000%
50	1.8491	1.8482	7.554	7.554
	center, bot.	center, bot.	(0,0), bot.	(0,0), bot.
	0.046%	0.000%	0.000%	0.000%
20	1.1554×10^{1}	1.1521×10^{1}	4.6934×10^{1}	4.6934×10^{1}
	center, bot.	center, bot.	(0,0), bot.	(0,0), bot.
	0.289%	0.000%	0.000%	0.000%
10	4.6202×10^{1}	4.5671×10^{1}	1.8379×10^{2}	1.8384×10^{2}
	center, bot.	center, bot.	(0,0), bot.	(0,0), bot.
	1.204%	0.042%	0.032%	0.005%
5	1.8793×10^{2}	1.7869×10^{2}	7.2738×10^{2}	7.1704×10^{2}
	center, bot.	center, bot.	(0,0), bot.	(0,0), bot.
	5.542%	0.350%	1.570%	0.127%
2	1.0761×10^{3}	8.9634×10^{2}	1.0455×10^{3}	1.3100×10^{3}
	center, 0.1	center, 0.2	(a/4,b/4), top	(a/4,b/4), top
	–	1.466%	–	–

Table 16 Minimum failure load amplitudes (N/mm^2), locations and absolute percentage errors for distributed loadings via HOTs$_{ee}$, N_f=2

a/h	Centric loading		Off-centric loading	
	N=3	N=4	N=3	N=4
100	4.6221×10^{-1}	4.6222×10^{-1}	1.8901	1.8901
	center, bot.	center, bot.	(0,0), bot.	(0,0), bot.
	0.001%	0.000%	0.000%	0.000%
50	1.8481	1.8482	7.5540	7.5540
	center, bot.	center, bot.	(0,0), bot.	(0,0), bot.
	0.006%	0.000%	0.000%	0.000%
20	1.1517×10^{1}	1.1521×10^{1}	4.6934×10^{1}	4.6934×10^{1}
	center, bot.	center, bot.	(0,0), bot.	(0,0), bot.
	0.036%	0.000%	0.000%	0.000%
10	4.5584×10^{1}	4.5652×10^{1}	1.8385×10^{2}	1.8385×10^{2}
	center, bot.	center, bot.	(0,0), bot.	(0,0), bot.
	0.148%	0.000%	0.000%	0.000%
5	1.7678×10^{2}	1.7803×10^{2}	7.1629×10^{2}	7.1612×10^{2}
	center, bot.	center, bot.	(0,0), bot.	(0,0), bot.
	0.721%	0.018%	0.021%	0.002%
2	8.9947×10^{2}	8.9656×10^{2}	1.1557×10^{3}	1.2363×10^{3}
	center, 0.3	center, 0.2	(a/4,b/4), 0.3	(a/4,b/4), 0.4
	–	1.442%	–	8.061%

Table 17 Minimum failure load amplitudes (N/mm^2), locations and absolute percentage errors for distributed loadings via HOTs$_{ee}$, N_l=4

a/h	Centric loading		Off-centric loading	
	N=3	N=4	N=3	N=4
100	4.6222×10^{-1}	4.6222×10^{-1}	1.8901	1.8901
	center, bot.	center, bot.	(0,0), bot.	(0,0), bot.
	0.000%	0.000%	0.000%	0.000%
50	1.8482	1.8482	7.554	7.554
	center, bot.	center, bot.	(0,0), bot.	(0,0), bot.
	0.000%	0.000%	0.000%	0.000%
20	1.1520×10^{1}	1.1521×10^{1}	4.6934×10^{1}	4.6934×10^{1}
	center, bot.	center, bot.	(0,0), bot.	(0,0), bot.
	0.004%	0.000%	0.000%	0.000%
10	4.5644×10^{1}	4.5652×10^{1}	1.8385×10^{2}	1.8385×10^{2}
	center, bot.	center, bot.	(0,0), bot.	(0,0), bot.
	0.018%	0.000%	0.000%	0.000%
5	1.7789×10^{2}	1.7806×10^{2}	7.1613×10^{2}	7.1613×10^{2}
	center, bot.	center, bot.	(0,0), bot.	(0,0), bot.
	0.098%	0.000%	0.001%	0.000%
2	9.0753×10^{2}	9.0904×10^{2}	1.3113×10^{3}	1.3727×10^{3}
	center, 0.2	center, 0.2	(a/4,b/4), 0.4	(a/4,b/4), 0.4
	0.236%	0.070%	2.483%	2.082%

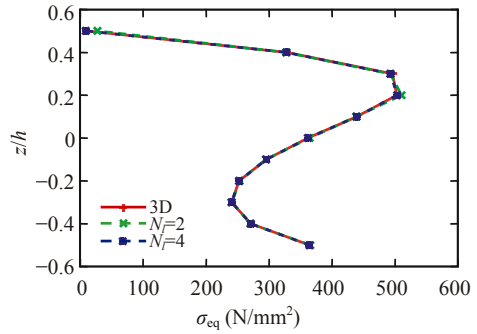

Fig.15 von Mises' stress along thickness at plate center via exact solution and LHOT, N=4, N_l=2 and 4 for centric loading equal to 3D failure load, a/h=2

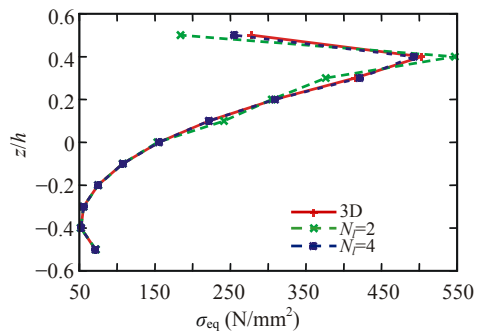

Fig.16 von Mises' stress along thickness at (a/4, b/4) via exact solution and LHOT, N=4, N_l=2 and 4 for off-centric loading equal to 3D failure load, a/h=2

off-centric loading. Figs.15 and 16 show the equivalent stress for very thick plates and centric and off-centric loadings, respectively. Due to the high stress gradient present at plate top, accuracy in the case of off-centric loading and very thick plates can be improved considering layers of appropriate thickness. Results shown in Table 18 have been obtained considering a fictitious layer for $0.35\leq z/h\leq0.5$. The remaining part of the plate has been divided into layers of equal thickness.

Table 18 Minimum failure load amplitudes (N/mm^2), locations and absolute percentage errors for distributed loadings via LHOTs$_{ee}$, a/h=2, layers of different thickness

N_l	Uniform loading	
	N=3	N=4
3	1.3630×10^{3}	1.3588×10^{3}
	(a/4,b/4), 0.4	(a/4,b/4), 0.4
	1.361%	1.049%
4	1.3612×10^{3}	1.3595×10^{3}
	(a/4,b/4), 0.4	(a/4,b/4), 0.4
	1.227%	1.101%

CONCLUSION

The failure analysis of isotropic, simply supported, square plates has been treated. Distributed and localized loadings' conditions have been considered. In the case of distributed loadings, attention has been focused on bi-sinusoidal and uniform loads. Centric and off-centric stepwise constant loads have been studied in the case of localized loadings. Minimum failure load amplitudes and locations have been considered. Also the von Mises' equivalent stress has been plotted along the plate thickness. The length-to-thickness ratio (a/h) has been chosen as analysis parameter in order to account for thin plates (a/h=100) as well as for very thick plates (a/h=2). Results have been obtained via the 3D exact model by Demasi (2007). That solution has shown that failure is experienced at plate center point in the case of bi-sinusoidal and centric stepwise loadings. In the case of a uniform failure load, the failure condition is reached first at the plate corners, due to the in-plane shear stress component. For the off-centric stepwise loading, failure is located at plate corner (0, 0) for $a/h\geq5$ and at the point (a/4, a/4) in the case of very thick plates. The presence of a high stress gradient in the case of uniform and off-centric stepwise loadings in the neighborhood of the plate top for a/h=2 have

been found. That represents a challenging condition in order to assess the addressed 2D models. The unified formulation by Carrera (2002; 2003) has been considered in order to formulate the 2D models. Those theories have been grouped into CTs that model the shear deformations (HOTs^{d}) or both the shear deformations and the transverse deformability (HOTs). Higher order theories (LHOTs) that permit splitting the plate domain into smaller fictitious layers are also considered. The polynomial approximation of the displacement field is applied at layer level. CTs yield highly accurate results for $a/h\geq10$ in the case of distributed loadings, with the percentage absolute error about being 0.5%. The same accuracy is obtained in the case of localized loadings for $a/h\geq20$. For thick plates the percentage error can be even as high as 6% and in the case of $a/h=2$ the failure locations are not correctly predicted. Third order HOT^{d} yields more accurate results than CTs for distributed loadings and $a/h=5$. The error is about 1%. Fourth order HOT yields results that match the exact solution for thick plates in the case of bi-sinusoidal and localized loadings. In the other considered loading conditions results obtained via HOTs are not accurate due to the presence of the high stress gradient. In that case the assumption of the LHOTs is required. It has been shown that via an appropriate choice of the mathematical interface a solution as accurate as wanted can be obtained, even in those cases where loading conditions are such as to yield complicated local stress states.

References

Carrera, E., 2002. Theories and finite elements for multilayered plates and shells. *Archives of Computational Methods in Engineering*, **9**(2):87-140. [doi:10.1007/BF02736649]

Carrera, E., 2003. Theories and finite elements for multilayered plates and shells: a unified compact formulation with numerical assessment and benchmarking. *Archives of Computational Methods in Engineering*, **10**(3):215-296. [doi:10.1007/BF02736224]

Carrera, E., Giunta, G., 2007. Hierarchical closed form solutions for plates bent by localized transverse loadings. *Journal of Zhejiang University SCIENCE A*, **8**(7):1026-1037. [doi:10.1631/jzus.2007.A1026]

Cauchy, A.L., 1828. Sur l'euilibre et le mouvement d'une plaque solide. *Exercises de Matematique*, **3**:328-355.

Demasi, L., 2007. 3D closed form solution and exact thin plate theories for isotropic plates. *Composites Structures*, **80**(2):183-195. [doi:10.1016/j.compstruct.2006.04.073]

Kam, T.Y., Jan, T.B., 1995. First-ply failure analysis of laminated composite plates based on the layerwise linear displacement theory. *Composites Structures*, **32**(1-4):583-591. [doi:10.1016/0263-8223(95)00069-0]

Kirchhoff, G., 1850. Über das Gleichgewicht und die Bewegung einer elastishen Sceibe. *J. Reine Angew. Math.*, **40**:51-88.

Librescu, L., 1975. Elasto-statics and Kinematics of Anisotropic and Heterogeneous Shell-type Structures. Nordhoff Int., Leiden, The Netherlands.

Love, A.E.H., 1959. A Treatise on Mathematical Theory of Elasticity. Cambridge University Press, UK.

Mindlin, E., 1951. Influence of the rotatory inertia and shear in flexural motions of isotropic elastic plates. *J. Appl. Mech.*, **18**:1031-1036.

Pandey, A.K., Reddy, J.N., 1987. A Post First-ply Failure Analysis of Composites Laminates. Structures, Structural Dynamics and Materials Conference, Monterey, CA, USA, p.788-797.

Poisson, S.D., 1829. Memoire sur l'euilibre et le mouvement des corps elastique. *Mem. Acad. Sci.*, **8**:357.

Reddy, J.N., 1984. A simple higher-order theory for laminated composite plates. *J. Appl. Mech.*, **51**:745-752.

Reddy, J.N., 1997. Mechanics of Laminated Composites Plates. Theory and Analysis. CRC Press, Boca Raton, Florida.

Reddy, J.N., Pandey, A.K., 1987. A first-ply failure analysis of composites laminates. *Computers and Structures*, **25**(3):371-393. [doi:10.1016/0045-7949(87)90130-1]

Reddy, Y.S.N., Reddy, J.N., 1987. Linear and Non Linear Failure Analysis of Composites Laminates with Transverse Shear. American Institute of Aeronautics and Astronautics, Inc.

Reissner, E., 1945. The effect of transverse shear deformation on the bending of elastic plates. *J. Appl. Mech.*, **12**:69-76.

Turvey, G.J., 1980a. An initial flexural failure analysis of symmetrically laminated cross-ply rectangular plates. *International Journal of Solids and Structures*, **16**(5):451-463. [doi:10.1016/0020-7683 (80)90043-8]

Turvey, G.J., 1980b. Flexural failure analysis of angle-ply laminates of GFRP and CFRP. *The Journal of Strain Analysis for Engineering Design*, **15**:43-49. [doi:10.1243/03093247V151043]

Turvey, G.J., 1980c. A study on the onset of flexural failure in cross-ply laminated strips. *Fibre Science and Technology,* **13**(5):325-336. [doi:10.1016/0015-0568(80)90008-1]

Turvey, G.J., 1981. Initial flexural failure of square, simply supported, angle-ply plates. *Fibre Science and Technology*, **15**(1):47-63. [doi:10.1016/0015-0568(81) 90031-2]

Turvey, G.J., 1982. Uniformly loaded, antisymmetric cross-ply laminated, rectangular plates: an initial flexural failure analysis. *Fibre Science and Technology*, **16**(1):1-10. [doi:10.1016/0015-0568(82)90010-0]

Turvey, G.J., 1987. Effect of Shear Deformation on the Onset of Flexural Failure in Symmetric Cross-ply Laminated Rectangular Plates. *In*: Marshall, I.H. (Ed.), Composites Structures. Elsevier Applied Science, London, p.141-146.

Washizu, K., 1968. Variational Methods in Elasticity and Plasticity. Pergamon Press, NY.